Contents lists available at ScienceDirect

Physics Letters B

www.elsevier.com/locate/physletb

Precise determination of lattice phase shifts and mixing angles

CrossMark

Bing-Nan Lu [a,*], Timo A. Lähde [a], Dean Lee [b], Ulf-G. Meißner [c,a,d]

[a] *Institute for Advanced Simulation, Institut für Kernphysik, and Jülich Center for Hadron Physics, Forschungszentrum Jülich, D-52425 Jülich, Germany*
[b] *Department of Physics, North Carolina State University, Raleigh, NC 27695, USA*
[c] *Helmholtz-Institut für Strahlen- und Kernphysik and Bethe Center for Theoretical Physics, Universität Bonn, D-53115 Bonn, Germany*
[d] *JARA – High Performance Computing, Forschungszentrum Jülich, D-52425 Jülich, Germany*

ARTICLE INFO

ABSTRACT

We introduce a general and accurate method for determining lattice phase shifts and mixing angles, which is applicable to arbitrary, non-cubic lattices. Our method combines angular momentum projection, spherical wall boundaries and an adjustable auxiliary potential. This allows us to construct radial lattice wave functions and to determine phase shifts at arbitrary energies. For coupled partial waves, we use a complex-valued auxiliary potential that breaks time-reversal invariance. We benchmark our method using a system of two spin-1/2 particles interacting through a finite-range potential with a strong tensor component. We are able to extract phase shifts and mixing angles for all angular momenta and energies, with precision greater than that of extant methods. We discuss a wide range of applications from nuclear lattice simulations to optical lattice experiments.

1. Introduction

Lattice methods are widely used in studies of quantum few- and many-body problems in nuclear, hadronic, and condensed matter systems, see *e.g.* Refs. [1–5]. A necessary step in such studies is the computation of scattering phase shifts and mixing angles from an underlying microscopic lattice Hamiltonian. Remarkably, the same problem arises in the context of experiments on optical lattices. Several groups have pioneered the use of ultracold atoms in optical lattices produced by standing laser waves, to emulate the properties of condensed matter systems and quantum field theories [6–10]. The basic concept is to tune the interactions of the atoms, both with each other and with the optical lattice, to reproduce the single-particle properties and particle–particle interactions of the "target theory". Such studies often require a more general setup than a simple cubic lattice, for instance in the case of the hexagonal Hubbard model [11], which closely resembles the physics of graphene [12] and carbon nanotubes [13]. Clearly, a robust and accurate method for computing scattering parameters on arbitrary lattices is needed.

For the scattering of particles on a cubic lattice, Lüscher's finite-volume method [14] uses periodic boundary conditions to infer elastic scattering phase shifts from energy eigenvalues. The method

has been widely used in lattice QCD simulations with applications to different angular momenta [15–19] as well as partial-wave mixing [20], see Ref. [2] for a recent review. An important advantage of Lüscher's method is that periodic boundary conditions are typically already used in lattice calculations of nuclear, hadronic, ultracold atomic, and condensed matter systems. Since no additional boundary constraints are needed, the method is easily applied to a wide class of systems.

However, Lüscher's method requires that the finite-volume energy levels can be accurately determined, with errors small compared to the separation between adjacent energy levels. This is not practical in cases such as nucleus–nucleus scattering, where the separation between finite-volume energy levels is many orders of magnitude smaller than the total energy of the system. Fortunately, this problem has been solved using an alternative approach called the adiabatic projection method [21–24]. There, initial cluster states are evolved using Euclidean time projection and used to calculate an effective two-cluster Hamiltonian (or transfer matrix). In the limit of large projection time, the spectral properties of the effective two-cluster Hamiltonian coincide with those of the original underlying theory. This method has been applied to nuclei and ultracold atoms, while applications to lattice QCD simulations of relativistic hadronic systems are currently being investigated.

Since the adiabatic projection method reduces all scattering systems to an effective two-cluster lattice Hamiltonian, additional boundary conditions can be applied to the effective lattice Hamiltonian in order to compute scattering properties. This opens the

---

* Corresponding author.
E-mail address: b.lu@fz-juelich.de (B.-N. Lu).

door to methods more accurate than Lüscher's by removing the effects of the periodic boundary conditions, which are otherwise a significant source of rotational symmetry breaking. One promising approach is to place the particles in a harmonic oscillator potential and extract phase shifts from the energy eigenvalues [25,26]. Another prominent example is the method used in Refs. [5,27], whereby a "spherical wall" is imposed on the relative separation between the two scattering particles. Phase shifts are then determined using the constraint that the wave function vanishes at the wall boundary. This method has been applied to the two-nucleon problem in lattice effective field theory (EFT) [28–31] and to lattice simulations of nucleus–nucleus scattering using the adiabatic projection method [21–24].

In spite of such progress in lattice scattering theory, all methods are still lacking in precision, especially when partial-wave mixing and high angular momenta are concerned. In previous work, numerical approximations were used for the study of coupled-channel systems [5]. We now describe an extension of the spherical wall method, which enables an efficient and precise determination of two-particle scattering parameters for arbitrary energies and angular momenta. We use angular momentum projection and solve the lattice radial equation with spherical wall boundaries, supplemented by an "auxiliary potential". We test our method on a lattice model with strong tensor interactions that induce appreciable partial-wave mixing. We expect our method to be applicable in theoretical lattice studies of nuclear, hadronic, ultracold atomic, and condensed matter systems, as well as in the experimental design of optical lattices. While we discuss only non-relativistic wave mechanics in our examples here, the extension to relativistic systems simply entails replacing the non-relativistic dispersion relation with the relativistic one.

2. Benchmark system

We begin with the eigenvalue equation

$$\left[-\frac{\nabla^2}{2\mu} + V(\mathbf{r}, \boldsymbol{\sigma}_1, \boldsymbol{\sigma}_2) \right] \psi = E\psi, \tag{1}$$

where $\mathbf{r}$ is the relative displacement, $\boldsymbol{\sigma}_i$, with $i = 1, 2$, are the spins of the two scattering nucleons with $m_N \equiv 2\mu = 938.92$ MeV. Following Ref. [5], we take

$$V = C \left\{ 1 + \frac{r^2}{R_0^2} \left[3(\hat{\mathbf{r}} \cdot \boldsymbol{\sigma}_1)(\hat{\mathbf{r}} \cdot \boldsymbol{\sigma}_2) - \boldsymbol{\sigma}_1 \cdot \boldsymbol{\sigma}_2 \right] \right\}$$
$$\times \exp\left(-\frac{r^2}{2R_0^2} \right), \tag{2}$$

with $C = -2.00$ MeV and $R_0 = 2.00 \times 10^{-2}$ MeV^{-1}. We only consider states of total intrinsic spin $S = 1$. The radial equation is

$$\left[-\frac{1}{2\mu r} \frac{\partial^2}{\partial r^2} r + \frac{L(L+1)}{2\mu r^2} + V_J(r) \right] \psi_J(r) = E\psi_J(r), \tag{3}$$

where L is the orbital angular momentum and J the total angular momentum. The "effective" potential is

$$V_J(r) = C\left(1 + \frac{2r^2}{R_0^2}\right) \exp\left(-\frac{r^2}{2R_0^2}\right), \tag{4}$$

for uncoupled channels, and

$$V_J(r) = C\left[1 + \frac{r^2}{R_0^2} \begin{pmatrix} -\frac{2(J-1)}{2J+1} & \frac{6\sqrt{J(J+1)}}{2J+1} \\ \frac{6\sqrt{J(J+1)}}{2J+1} & -\frac{2(J+2)}{2J+1} \end{pmatrix} \right]$$
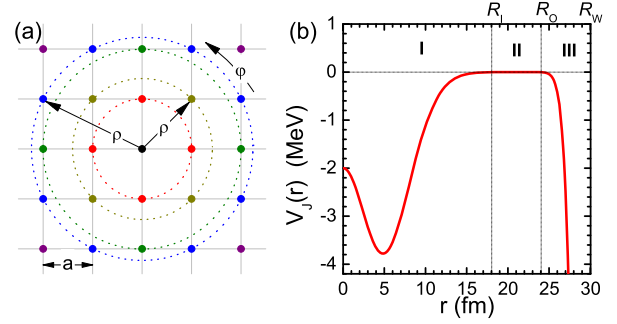$$\times \exp\left(-\frac{r^2}{2R_0^2}\right), \tag{5}$$

Fig. 1. (Color online.) Left panel: Grouping of mesh points according to lattice coordinates (ρ, φ), with lattice spacing a. Right panel: Spherical wall radius R_W, interaction regions I–III as discussed in the text and effective potential $V_J(r)$ for uncoupled channels with $V_0 = -25$ MeV.

for coupled ones. In the continuum, phase shifts and mixing angles are obtained by solving Eq. (3) using the potentials (4) and (5) with appropriate boundary conditions.

As rotational symmetry is broken by the lattice, the energy eigenstates of Eq. (1) belong to the irreducible representations (*irreps*) A_1, A_2, E, T_1 and T_2 of the cubic group $SO(3, Z)$ rather than the full $SO(3)$ rotational group [5,32,33]. For cubic periodic boundary conditions, as in Lüscher's method [14], the cubic symmetry remains exact, thus our solutions can still be classified by cubic *irreps*. Nevertheless, the rotational symmetry breaking due to the boundaries makes it difficult to identify states of high angular momentum and to extract scattering parameters. In order to remove these effects, we impose a hard spherical wall of radius R_W,

$$V \to V + \Lambda\theta(r - R_W), \tag{6}$$

where θ is the Heaviside step function and Λ is a (large) positive constant, intended to sufficiently suppress the wave function beyond R_W (we set $\Lambda = 10^8$ MeV). We take R_W to exceed the range of the interaction, such that the boundary is placed in the asymptotic (non-interacting) region. We also take $2R_W$ to be less than the difference of the box size and the interaction range, which ensures that cubic boundary effects remain negligible.

3. Angular momentum decomposition

Let $|\vec{r}\rangle \otimes |S_z\rangle$ denote a two-body quantum state with separation $\vec{r}$ and z-component of total intrinsic spin S_z. We define radial lattice coordinates (ρ, φ) by grouping equidistant mesh points, as shown in Fig. 1. To construct radial wave functions, we project onto states with total angular momentum (J, J_z) in the continuum limit, using

$$|m\rangle_{(L)}^{(J),(J_z)} \equiv \sum_{\vec{n}, L_z, S_z} C_{L, L_z, S, S_z}^{J, J_z} Y_{L, L_z}(\hat{n})$$
$$\times \delta_{\rho_m, |\vec{n}|} |\vec{n}\rangle \otimes |S_z\rangle, \tag{7}$$

where the Y_{L, L_z} are spherical harmonics with orbital angular momentum (L, L_z). The $C_{L, L_z, S, S_z}^{J, J_z}$ are Clebsch–Gordan coefficients. The parentheses around J, J_z and L on the left hand side signify that these quantum numbers are not exactly good quantum numbers. Note that Eq. (7) is applicable to arbitrary geometries. Here, $\vec{n}$ runs over all lattice points and the "radial shell" is given by the integer m. Then, ρ_m is the distance from the origin in units of the lattice spacing a, and $\delta_{\rho_m, |\vec{n}|}$ picks out all lattice points for which $\rho_m = |\vec{n}|$. It may be practical (especially for non-cubic lattices) to relax this condition to include all lattice points with $||\rho_m - |\vec{n}|| < \delta$ for small, positive δ. On the lattice, the $|m\rangle_L^{J, J_z}$ form a complete

Table 1

Energy levels and differences Δ (in MeV) with (w/) and without (w/o) unphysical J-mixing matrix elements. In the former case, we compute the eigenstates of the lattice Hamiltonian without a spherical harmonic projection.

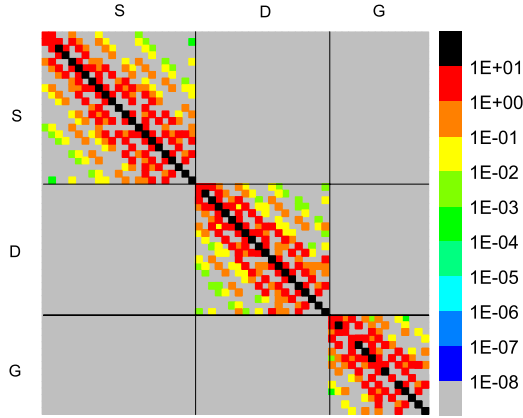| Even parity					Odd parity				
state	irrep	w/	w/o	Δ	state	irrep	w/	w/o	Δ
$1^3S(D)_1$	T_1	0.037	0.038	0.001	1^3P_1	T_1	0.917	0.918	0.001
1^3D_2	E	2.764	2.766	0.002	$1^3P(F)_2$	E	1.795	1.796	0.001
$1^3D(G)_3$	T_1	3.347	3.351	0.004	1^3P_0	A_1	3.048	3.053	0.005
1^3G_4	A_1	6.562	6.567	0.005	1^3F_3	A_2	4.616	4.620	0.004
1^3G_4	T_1	6.624	6.637	0.013	$1^3F(H)_4$	A_1	4.998	5.003	0.005

Fig. 2. (Color online.) Illustration of rotational symmetry breaking effects in the Hamiltonian matrix, given in the basis of Eq. (7). The colors show the magnitude of the matrix elements. To study unphysical mixings, we remove the tensor component of $V_J(r)$. The resulting Hamiltonian matrix should ideally be block-diagonal in the S-, D- and G-waves *etc.* Clearly, the matrix elements that cause unphysical mixings are suppressed by several orders of magnitude. In each block, the row and column indices represent the radial coordinates of the mesh points. For higher partial waves, entire "radial shells" ρ_m vanish due to the angular dependence of the wave function, and such redundant rows and columns have been removed.

(but non-orthonormal) basis. We therefore compute the norm matrix of these states before solving for the eigenstates of the lattice Hamiltonian.

We find that rotational symmetry breaking is almost entirely due to the non-zero lattice spacing a. As we take $a \to 0$ at fixed R_W, rotational symmetry is exactly restored. The degree of mixing between different total angular momenta J and J' is a useful indicator of rotational symmetry breaking. Such effects can be interpreted as arising from the non-orthogonality of wave functions in different partial waves when their inner product is computed as a sum over discrete lattice points. The degree of mixing is difficult to estimate *a priori*, as it depends strongly on the details of the interaction.

Given a simple cubic lattice with a cubic-invariant interaction, unphysical J-mixing only occurs between cubic *irreps* of the same type. If the objective is to describe a rotationally invariant system on the lattice, then we may simply drop all unphysical couplings between channels with different J. We find that rotational symmetry breaking is numerically insignificant at low energies in the spherical wall method. Still, it is instructive to study the sizes of the unphysical J-mixings. For this purpose, we use a simple cubic lattice with $a = 100$ MeV^{-1} and $R_W = 10.02a$. In the radial basis (7), the Hamiltonian matrix becomes nearly block-diagonal, with each block corresponding to a specific J. The non-block-diagonal elements induce unphysical J-mixing. In Table 1, we examine the lowest energy levels with and without J-mixing matrix elements. When J-mixing is included, we solve directly for the eigenstates of the lattice Hamiltonian without a spherical harmonic projection. In Fig. 2, we show the Hamiltonian matrix elements in the projected basis defined in Eq. (7). In order to focus entirely on

unphysical mixings caused by rotational symmetry breaking, we have neglected the tensor component of $V_J(r)$ in Fig. 2. The magnitude of such unphysical mixing matrix elements is found to be greatly suppressed.

4. Auxiliary potential

We first consider uncoupled channels, where V vanishes beyond an "inner" radius R_I. A hard wall at R_W gives access to discrete energy eigenvalues only, and a very large box is needed at low energies. To resolve these issues, we define an "outer" radius R_O, between R_I and R_W, as shown in Fig. 1. We also introduce a Gaussian "auxiliary" potential in region III,

$$V_{\text{aux}}(r) \equiv V_0 \exp\left[-(r - R_W)^2/a^2\right], \tag{8}$$

with $R_O \leq r \leq R_W$, where the separation between R_O and R_W is chosen such that V_{aux} is negligible at R_O. Note that V_{aux} vanishes in regions I and II. The energy eigenvalues can now be adjusted continuously as a function of V_0. In Fig. 1, we show $V_J(r)$ for $V_0 = -25$ MeV.

In order to extract phase shifts, we express $\psi(r)$ in region II as

$$\psi(r) \cong A h_J^-(kr) - B h_J^+(kr), \tag{9}$$

for $R_I \leq r \leq R_O$, where $h_J^+(kr)$ and $h_J^-(kr)$ are spherical Bessel functions, and $k = \sqrt{2\mu E}$. The constants A and B can be determined *e.g.* by a least-squares fit in region II. We note that

$$B = SA, \tag{10}$$

with $S \equiv \exp(2i\delta_J)$, from which δ_J can be obtained.

For coupled channels, ψ has two components with $L = J \pm 1$. Given Eq. (5), both satisfy the spherical Bessel equation in region II, and are therefore of the form (9). If we denote $A \equiv (A_{J-1}, A_{J+1})^T$ and $B \equiv (B_{J-1}, B_{J+1})^T$, the S-matrix couples channels with $L = J \pm 1$. In the Stapp parameterization [34],

$$S \equiv \begin{bmatrix} \exp(i\delta_{J-1}) & \\ & \exp(i\delta_{J+1}) \end{bmatrix}$$
$$\times \begin{bmatrix} \cos(2\epsilon_J) & i\sin(2\epsilon_J) \\ i\sin(2\epsilon_J) & \cos(2\epsilon_J) \end{bmatrix}$$
$$\times \begin{bmatrix} \exp(i\delta_{J-1}) & \\ & \exp(i\delta_{J+1}) \end{bmatrix}, \tag{11}$$

where ϵ_J is the mixing angle.

When solving S from Eq. (10) as in the uncoupled case, we encounter a subtle problem. For a simple hard wall boundary, only one independent solution per lattice energy eigenvalue is obtained. In order to determine S unambiguously, two linearly independent vectors A and B are needed. In Ref. [5], this problem was circumvented by taking two eigenfunctions with approximately the same energy and neglecting their energy difference. However, such a procedure introduces significant uncertainties.
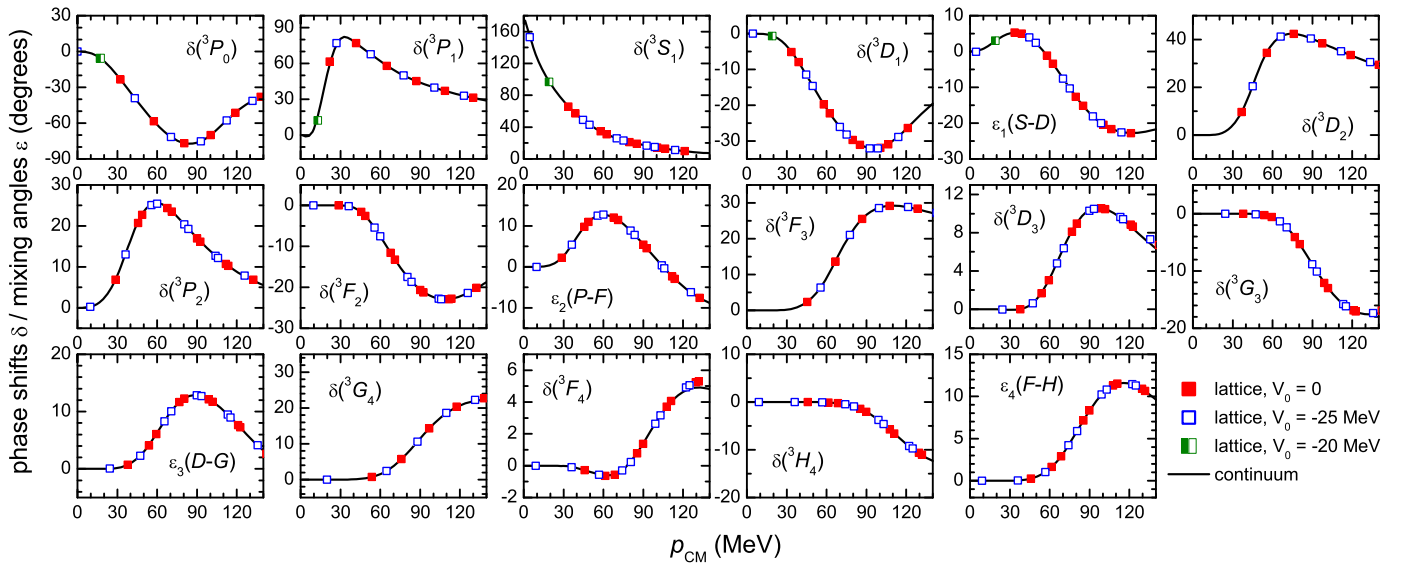
Fig. 3. (Color online.) Phase shifts and mixing angles for $J \leq 4$ and $S = 1$. Full, open and "half-open" squares correspond to $V_0 = 0$, $V_0 = -25$ MeV and $V_0 = -20$ MeV, respectively. For $V_0 = -20$ MeV, only partial results are shown in order to reduce clutter. Solid lines denote continuum results.

As the potential (5) is real and Hermitian, an exact time-reversal symmetry results. We now add to $V_J(r)$ an imaginary component,

$$V_J(r) \rightarrow V_J(r) + \begin{bmatrix} & iU_{\text{aux}}(r) \\ -iU_{\text{aux}}(r) & \end{bmatrix}, \qquad (12)$$

where $U_{\text{aux}}(r)$ is an arbitrary, real-valued function with support in region III only. This leaves $V_J(r)$ Hermitian and the energy eigenvalues real, while the time-reversal symmetry is broken. Also, ψ and ψ^* are now linearly independent and satisfy Eq. (3) in regions I and II with identical energy eigenvalues. In addition to Eq. (10), we have the conjugate expression,

$$A^* = SB^*, \qquad (13)$$

and the S-matrix

$$S = \begin{bmatrix} B & A^* \end{bmatrix} \begin{bmatrix} A & B^* \end{bmatrix}^{-1}, \qquad (14)$$

from (10) and (13). Phase shifts and mixing angles can then be obtained from Eq. (11). Note that the inverse in Eq. (14) cannot be computed without $U_{\text{aux}}(r)$, since in that case $A = -B^*$. We use

$$U_{\text{aux}}(r) = U_0 \, \delta_{r,r_0}, \qquad (15)$$

for $R_O \leq r_0 \leq R_W$, where r_0 is a radial mesh point in region III and U_0 is an arbitrary real constant. We find that the distortion of the energy eigenvalues and radial wave function introduced by this choice is minimal. The same methodology we have applied here for coupled partial waves can also be applied to more general problems with different scattering constituents.

5. Numerical results

We benchmark our method numerically with the interaction (2) using a cubic lattice with $a = 100$ MeV^{-1} ($\pi/a = 314$ MeV), box size $35a$, and we take $R_I = 9.02a$, $R_O = 12.02a$, and $R_W = 15.02a$. For all channels, we use the real auxiliary potential (8), while for coupled channels we add the complex auxiliary potential (15) with $U_0 = 20.0$ MeV and $r_0 \simeq R_W$.

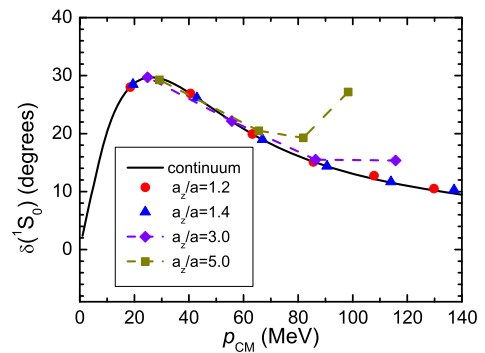In Fig. 3, we show our lattice phase shifts and mixing angles. We compare with continuum results, obtained by solving

Fig. 4. (Color online.) Phase shift for the $^1S_0$ channel on anisotropic rectangular lattices. Circles, triangles, diamonds and squares denote results for lattice spacings $a_z = 1.2a$, $a_z = 1.4a$, $a_z = 3.0a$ and $a_z = 5.0a$, respectively. The dashed lines are intended as a guide to the eye.

the Lippmann–Schwinger equation for each channel. All our lattice results agree well with the continuum ones, from threshold to a relative center-of-mass momentum of $p_{\text{CM}} \equiv k = 140$ MeV. We note the marked improvement over Ref. [5] for the same benchmark system.

6. Application to arbitrary lattices

While Lüscher's method has been extended to asymmetric rectangular boxes [35], no standard method yet exists for an arbitrary lattice. Our method can be used to characterize particle–particle interactions on arbitrary lattices, in any number of spatial dimensions. This is significant for optical lattices, as the lattice geometry is then engineered to reproduce the single-particle energies of a given condensed matter or quantum field theoretical system. Anisotropic lattices exhibit more breaking of rotational invariance than a simple cubic lattice does. This is often an essential feature, *e.g.* in the crossover from a three-dimensional system to a layered two-dimensional one. In Fig. 4, we show the $^1S_0$ phase shift on an anisotropic rectangular lattice, where the spacing along the z axis, a_z, exceeds those along the x and y axes, denoted collectively by a. The unit cell volume is 100^3 MeV^{-3} in all cases. While we find good agreement with the continuum up to $a_z \simeq 1.4a$, this

breaks down when a_z becomes comparable to the range of the interaction, with increasing deviation at high p_{CM}. Such a crossover to two-dimensional behavior can be characterized in terms of mixing between the $^1S_0$ and $^1D_2$ ($J_z = 0$) partial waves, an effect of rotational symmetry breaking. The low-energy particle–particle interactions of any lattice system can be similarly described.

7. Summary and discussion

We have described a general and systematic method for the calculation of scattering parameters on arbitrary lattices, which we have benchmarked using a lattice model of a finite-range interaction with a strong tensor component. Extensions to more general interactions are straightforward. The Coulomb interaction can be accounted for by replacing the spherical Bessel functions by Coulomb functions, and by defining the distance between particles as the minimum distance on a periodic lattice. The spherical wall then removes unphysical boundary effects. When combined with the adiabatic projection method, the techniques we have discussed can be applied to any scattering system in nuclear, hadronic, ultracold atomic, or condensed matter physics. We expect our method to be applicable to optical lattice experiments, in addition to its immediate usefulness for lattice studies in nuclear, hadronic, and condensed matter theory. In fact, the method proposed here has already been used to significantly improve the adiabatic projection method, as detailed in Ref. [36].

References

[1] D. Lee, Prog. Part. Nucl. Phys. 63 (2009) 117.
[2] J.E. Drut, A.N. Nicholson, J. Phys. G 40 (2013) 043101.
[3] J.-W. Chen, D.B. Kaplan, Phys. Rev. Lett. 92 (2004) 257002.
[4] B. Borasoy, E. Epelbaum, H. Krebs, D. Lee, U.-G. Meißner, Eur. Phys. J. A 31 (2007) 105.
[5] B. Borasoy, E. Epelbaum, H. Krebs, D. Lee, U.-G. Meißner, Eur. Phys. J. A 34 (2007) 185.
[6] J.P. Hague, C. MacCormick, Phys. Rev. Lett. 109 (2012) 223001.
[7] J.P. Hague, C. MacCormick, arXiv:1506.04005 [physics.atom-ph].
[8] X. Li, W. Vincent Liu, arXiv:1508.06285 [cond-mat.quant-gas].
[9] D. Banerjee, et al., Phys. Rev. Lett. 110 (2013) 125303.
[10] Y. Kuno, et al., New J. Phys. 17 (2015) 063005.
[11] Z.Y. Meng, et al., Nature 464 (2010) 847.
[12] P.V. Buividovich, M.I. Polikarpov, Phys. Rev. B 86 (2012) 245117.
[13] T. Luu, T.A. Lähde, Phys. Rev. B 93 (2016) 155106.
[14] M. Lüscher, Commun. Math. Phys. 105 (1986) 153.
[15] V. Bernard, M. Lage, U.-G. Meißner, A. Rusetsky, J. High Energy Phys. 08 (2008) 024.
[16] T. Luu, M.J. Savage, Phys. Rev. D 83 (2011) 114508.
[17] M. Göckeler, et al., Phys. Rev. D 86 (2012) 094513.
[18] N. Li, C. Liu, Phys. Rev. D 87 (2013) 014502.
[19] R.A. Briceño, Z. Davoudi, T.C. Luu, Phys. Rev. D 88 (2013) 034502.
[20] R.A. Briceño, Z. Davoudi, T. Luu, M.J. Savage, Phys. Rev. D 88 (2013) 114507.
[21] M. Pine, D. Lee, G. Rupak, Eur. Phys. J. A 49 (2013) 151.
[22] S. Elhatisari, D. Lee, Phys. Rev. C 90 (2014) 064001.
[23] A. Rokash, et al., Phys. Rev. C 92 (2015) 054612.
[24] S. Elhatisari, et al., Nature 528 (2015) 111.
[25] T. Luu, M.J. Savage, A. Schwenk, J.P. Vary, Phys. Rev. C 82 (2010) 034003.
[26] I. Stetcu, J. Rotureau, B. Barrett, U. Van Kolck, Ann. Phys. 325 (2010) 1644.
[27] J. Carlson, V.R. Pandharipande, R.B. Wiringa, Nucl. Phys. A 424 (1984) 47.
[28] B. Borasoy, E. Epelbaum, H. Krebs, D. Lee, U.-G. Meißner, Eur. Phys. J. A 35 (2008) 343.
[29] E. Epelbaum, H. Krebs, D. Lee, U.-G. Meißner, Eur. Phys. J. A 41 (2009) 125.
[30] E. Epelbaum, H. Krebs, D. Lee, U.-G. Meißner, Eur. Phys. J. A 45 (2010) 335.
[31] E. Epelbaum, H. Krebs, D. Lee, U.-G. Meißner, Phys. Rev. Lett. 104 (2010) 142501.
[32] R.C. Johnson, Phys. Lett. B 114 (1982) 147.
[33] B.-N. Lu, T.A. Lähde, D. Lee, U.-G. Meißner, Phys. Rev. D 90 (2014) 034507.
[34] H.P. Stapp, T.J. Ypsilantis, N. Metropolis, Phys. Rev. 105 (1957) 302.
[35] X. Li, et al., CLQCD Collaboration, J. High Energy Phys. 0706 (2007) 053.
[36] S. Elhatisari, D. Lee, Ulf-G. Meißner, G. Rupak, Eur. Phys. J. A 52 (6) (2016) 174.